



HAL
open science

Carbon/polyamide 6 thermoplastic composite cylinders for deep sea applications

Mael Arhant, Christophe Briançon, Christian Burtin, Peter Davies

► **To cite this version:**

Mael Arhant, Christophe Briançon, Christian Burtin, Peter Davies. Carbon/polyamide 6 thermoplastic composite cylinders for deep sea applications. *Composite Structures*, 2019, 212, pp.535 - 546. 10.1016/j.compstruct.2019.01.058 . hal-03485855

HAL Id: hal-03485855

<https://hal.science/hal-03485855>

Submitted on 20 Dec 2021

HAL is a multi-disciplinary open access archive for the deposit and dissemination of scientific research documents, whether they are published or not. The documents may come from teaching and research institutions in France or abroad, or from public or private research centers.

L'archive ouverte pluridisciplinaire **HAL**, est destinée au dépôt et à la diffusion de documents scientifiques de niveau recherche, publiés ou non, émanant des établissements d'enseignement et de recherche français ou étrangers, des laboratoires publics ou privés.



Distributed under a Creative Commons Attribution - NonCommercial 4.0 International License

CARBON/POLYAMIDE 6 THERMOPLASTIC COMPOSITE CYLINDERS FOR DEEP SEA APPLICATIONS

Mael Arhant¹, Briançon Christophe², Burtin Christian³, Peter Davies¹

¹IFREMER, Marine Structures Laboratory,
Centre de Bretagne, F-29280, France

²CETIM
Technocampus EMC2, F-44340 Bouguenais, France

³Ecole Centrale de Nantes,
Institut de Recherche en Génie Civil et Mécanique (GeM), F-44321 Nantes, France

Keywords: Thermoplastic, Polyamide, Carbon fibres, Buckling, Implosion

Abstract

The composite materials used at sea are today nearly all based on thermoset resins (polyester, epoxy). However, there is an increasing number of thermoplastic matrix polymers available on the market (PP, PA, PPS, PEEK...), which offer possibilities for forming by local heating, attractive mechanical properties and the potential for end of life recycling. The aim of this study was to design, manufacture and test thermoplastic composite pressure vessels for 4500 meter depth, in order to establish a technical, economic and ecological assessment of the use of these materials to replace traditional composites underwater. First, finite element calculations have been carried out to optimize the stacking sequence with respect to the external pressure and buckling resistance. Thick thermoplastic cylinders were then manufactured and tested until implosion, their behaviour showed a good agreement with calculations. Overall, the results show that it is possible to use Carbon/Polyamide 6 (C/PA6) thermoplastic composite cylinders for deep sea applications, as implosion pressures higher than 600 bar (6000 meter depth) were achieved.

1. Introduction

More than 70% of the oceans remain unexplored and in order to reach these unexplored areas, it is necessary to design exploration and monitoring devices that are able to withstand high hydrostatic pressures. For many years, metals have been used underwater. However, due to their excellent specific properties, composite materials are

starting to replace existing deep sea structures. The use of composites for pressure hulls of underwater vehicles and submarines has been an ongoing research topic for many years, since early work in the UK by Smith and colleagues in the 1970's [1]. Over the last 30 years, some metallic pressure hulls have been replaced by composite materials, particularly for unmanned submersibles vehicles [2,3], and in the military area composites are also widely used [4]. Over the years, various US Navy and ONR (Office of Naval Research) programmes and several European projects (e.g. EUCLID RTP 3.8, DEVILS, MAST-AUV, MAST-Composite Housings), have resulted in a solid database of test results from implosion studies on a range of materials and geometries [5-7]. Several academic studies have worked on the performance and the optimization of these pressure vessels underwater [8,9]. These have included buckling [10,11], failure envelope determination [12-14], post buckling behaviour [15], and studies of winding angles [16].

Most of the composite materials used today in a marine environment are thermoset-based composites (polyester, epoxy). The pressure vessels, initially manufactured by filament winding, require high thicknesses (more than 10 mm) and obtaining such thicknesses without defects is a challenge; residual stresses and delaminations upon curing are common and can lead to premature failures. Moreover, these structures require long curing cycles that can be a limit in the industry.

To limit these long curing cycles, an increasing number of thermoplastic matrix polymers are available on the market (PP, polyamide, PPS, PEEK, PEKK...), which offer possibilities for forming by local heating, attractive mechanical properties, good environmental resistance, the potential for end of life recycling and manufacturing times several orders of magnitude faster than their thermoset counterpart. More ductile, and repairable by melting, they offer a potential for greatly improved devices. From a scientific point of view, most of the previous studies conducted on these materials were focused on aircraft structures, i.e. thin composite structures, and several studies have made connections between manufacture and microstructure [17-19].

Nonetheless, results concerning thermoplastic composite cylinders subjected to hydrostatic pressure are quite rare. A study in the USA on Carbon/PEEK (C/PEEK) was described by Gruber et al. [20]. At Ifremer, studies were performed from 2000 onwards, to examine different thermoplastic matrix polymers for underwater cylinders [21]. These tubes were supplied by American companies, first small diameter (55mm, 6mm wall thickness) then larger (175 mm diameter, 20 mm thick). Two were retained for hydrostatic pressure testing, carbon/PEEK and glass/PEI. The former were very promising, implosion pressures were similar to those obtained for carbon/epoxy, while the latter suffered from poor manufacturing quality (high porosity) and imploded at much lower pressures than glass/epoxy of similar geometry. Concerning offshore applications,

considerable work has been performed on long tubular composites both for risers and other flow-lines. Early work by IFP and Aerospatiale [22] in the 1980's was followed by various other projects over the last 25 years [23-26] to develop thermoset composite tubes with metal liners, and the publication of guidelines by the DNV [27]. Other groups have focused on thermoplastic matrix composites, in particular the Dutch company Airborne [28] which supplies down-lines for sub-sea intervention with various thermoplastic polymers and the **British company Magma [29] which is developing piping products made of C/PEEK composites.**

These structures **can be** manufactured by **Automated** Tape Placement (ATP), a process firstly developed in the 1960s for thermosets and then been adapted later for thermoplastic composites [28]. It uses narrow bands (tapes) of prepregs (typically 1 inch, ½ inch or ¼ inch wide) that are laid ply-by-ply on a mandrel or surface (flat or curved). These are consolidated upon deposition using a compaction roller. Intimate contact between the plies is ensured by a local increase of the tape temperature.

For many years, this process has been studied in detail in the industry and in academic studies [31-35], however, it is only today that this process is starting to reach its full maturity, with the help of a new generation of machines using near infra-red (NIR) high power diode lasers called Laser **assisted Automated** Tape Placement (LATP) machines. At first, difficulties were highlighted when trying to reach the mechanical properties obtained by autoclave using CO₂ lasers and hot gas torch heating systems. An excellent compilation of this was recently published by Stokes-Griffin [36] in which the interlaminar shear strength of C/PEEK composites manufactured by ATP was compared as a function of the different generations of machines used throughout the years. It shows the evolution in mechanical properties obtained using different generations of machines compared to the autoclave reference, highlighting the efficiency of today's machines, both in terms of mechanical properties and also placement rates.

The objective of the current study is to manufacture thick thermoplastic composite cylinders (over 10 mm) by **LATP** that can resist high hydrostatic pressures (above 450 bars). Their behaviour will be compared to that of existing carbon/epoxy cylinders used at Ifremer for deep sea applications. These are 1.2 meters long, have an inner diameter of 120 mm and a thickness of 12 mm. In the literature, a significant amount of work has been reported concerning C/PEEK composites. However, for the application of interest, i.e., oceanographic applications, these are very expensive, so cheaper thermoplastics (Polyamide 6) have been investigated here. To the knowledge of the authors, no work is currently available in the literature concerning the implosion of C/PA6 composites cylinders. The aim of this study is also to try and predict the implosion pressures of these materials, even if this subject is known to be difficult, as demonstrated by the World-wide failure exercise [12].

This work is also part of a project that included the durability of such hydrophilic polymers. It is not clear what their durability will be in such harsh environments when using such high thicknesses (> 10 mm). Understanding and being able to predict the effect of prolonged deep sea immersion on both the water diffusion and the mechanical properties is essential when long service lives (several years) are considered. This has been addressed in recent research papers on the subject, in which a specific water diffusion model for Polyamide 6 has been proposed [37], and used to predict the evolution in mechanical properties in the neat Polyamide 6 [38]. This was then extended to Carbon/Polyamide 6 in [39]. These results will be used at the end of this paper to **examine** the effect of water on the C/PA6 composite cylinders used in this study.

2. Materials and Methods

2.1. Materials

The material of interest here is a C/PA6 pre-impregnated tape from Celanese® (reference: CFR-TP PA6 CF60-01). It has a thickness of 190 µm (information given by the supplier), a fibre volume fraction of $48 \pm 1 \%$ and a density of $1.46 \pm 0.01 \text{ g.cm}^{-3}$. No information was provided by the supplier related to the type of fibre or about the polymer grade. The thermoplastic composite cylinders were compared to a carbon/epoxy used at sea at Ifremer for deep sea applications. It is a commercial wet filament wound carbon/epoxy (C/Epoxy) cylinder and is made of HTS45 fibres and a proprietary epoxy matrix. It has a fibre volume fraction of $61.5 \pm 1.5 \%$ and a density of $1.52 \pm 0.01 \text{ g.cm}^{-3}$. Fibre weight fractions were determined from matrix burn-off tests, which were performed by thermogravimetric analysis (TGA) at 450°C for 2 hours under a constant flux of N₂ to prevent oxidation of the carbon fibres. These were coupled with density measurements performed using a gas pycnometer in order to estimate fibre volume fractions.

2.2. Manufacturing process

In 2013, the CETIM (Technical Centre of the Mechanical Industries), located in Nantes (France), invested in an LAMP machine. This machine uses a Kuka robot coupled with an AFPT placement head, as shown in Figure 1.

Figure 1: *C/PA6 Thermoplastic cylinder manufactured by LATP at CETIM composite manufacturing facility using Kuka robot and AFPT heating head*

Three different composite cylinders have been investigated here. First, the C/Epoxy reference was produced by wet filament winding with a $[\pm 55^\circ]_{31}$ lay-up relative to the tube axis. Second, two C/PA6 thermoplastic composite cylinder were manufactured by LATP. The first was manufactured at $[\pm 55^\circ]_{31}$ in order to compare with the C/epoxy reference. The second was manufactured using an optimised sequence $[0^\circ/\pm 88^\circ]_{26}$. It has been shown and stated several times in the literature that this sequence should perform better than the $[\pm 55^\circ]$ sequence when subjected to hydrostatic pressures [11].

The dimensions, sequences and geometry of the different composite cylinders are given in Table 1.

Table 1: *Dimensions and geometry of the cylinders tested during this work*

The first two cylinders were manufactured on a 120 mm diameter mandrel and the third one was manufactured using a mandrel of 100 mm diameter. The third cylinder, laid at $[0^\circ/\pm 88^\circ]$, was manufactured with reinforcements at both ends to prevent failure at this location. The process parameters used to manufacture the thermoplastic cylinder are shown in Table 2. These were optimised overtime following the reception of the LATP machine by the CETIM. The processing temperature was optimised using an infrared camera close to the laser head that allowed parameters to be adjusted in order to obtain an homogeneous temperature field throughout the process. Moreover, that for the application of interest, i.e. deep sea structure, the loading is of a compressive nature, and it is clear that for these applications the fibres need to be straight to avoid microbuckling; this is known to limit the compressive properties.

Table 2: *Process parameters used for manufacturing thermoplastic composite cylinders*

2.3. Mechanical tests

Two types of mechanical test have been performed, in order to assess the performance of the three cylinders: axial compression tests on a electromechanical test machine of 200 kN capacity and implosion tests performed in a pressure vessels of 2400 bar capacity.

2.3.1. Instrumentation

Strain gauges were bonded around the perimeter at the centre of the cylinders, as shown in Figure 2. Using this number of strain gauges allows the determination of whether the cylinder implodes due to buckling or due to material failure.

Figure 2: Strain gauge configurations used for the composite cylinders (a) C/Epoxy [$\pm 55^\circ$] and C/PA6 [$\pm 55^\circ$]
(b) C/PA6 [$0^\circ/\pm 88^\circ$]

2.3.2. Axial Compression tests

Prior to each implosion test, an axial compression test was performed on each cylinder to measure the axial elastic properties (E_z and ν_{z0}) and check the response of all the strain gauges, as shown on Figure 3. Each cylinder was subjected to a small axial strain, around 1000 microstrain. Each tube was rotated and tested in different positions to ensure that loading was uniform and an average was then calculated. It should be noted that due to the large cross-section this test required an axial load of several tons.

Figure 3: *Axial compression test performed on a C/PA6 thermoplastic cylinder*

2.3.3. Implosion tests

All cylinders were then tested to implosion in a 2400 bar capacity pressure vessel with continuous recording of pressure, temperature and strain gauge measurements. The pressure was increased at 12 bar/min until failure. The pressure vessel is shown in Figure 4 together with the C/PA6 cylinder just before test.

Figure 4: *2400 bar pressure used for implosion test showing the 100 mm diameter C/PA6 cylinder just before test*

For each implosion test, aluminium end covers were bonded to the cylinder extremities in order to protect the ends and provide a suitable surface to seal the end plates. Then, the strain gauges were protected from

water and connected to the recording system. Each end fixture is specifically designed and machined for a given cylinder.

2.4. Finite Element Modelling

Finite element calculations have been performed in order to analyse the implosion test on the C/PA6 cylinder laid at $[0^\circ/\pm 88^\circ]$ and at $[\pm 55^\circ]$ using the commercially available software AbaqusTM. The mechanical properties used for the finite element calculations are shown in Table 3. Most of the mechanical properties were measured on composite panels manufactured by thermo-compression from the same fibres and matrix, within the project [39].

Table 3: *Mechanical properties used in the modelling stage for the C/PA6 cylinders, from [39], *calculated using laminate theory, not measured*

The composite cylinders are meshed using hexahedron elements (type C3D8R), with 7 through thickness elements of 5 mm, Figure 5.a. The end covers are also meshed using hexahedron elements of 8 mm, Figure.5.b.

Figure 5: *Mesh conditions using hexahedron elements for the $[0^\circ/\pm 88^\circ]$ composite cylinder, type C3D8R elements (a) Composite tube (b) End fixtures*

The interface between the composite tube and the end covers is considered without friction. The tube and the end fixtures are blocked in axial displacement in order to avoid rigid body movements without affecting the external pressure. The pressure is applied on the lateral faces of the end plates and on the external surface of the composite cylinder. An axial load is also applied and equal to the hydrostatic pressure divided by the end cover section. **To illustrate this, a schematic representation of the boundary conditions is shown in Figure 6.**

Figure 6: *Pressure conditions used for modelling*

3. Results and Discussion

3.1. Quality control (Ultrasonic C-Scan and X-Ray tomography)

Ultrasound inspection is of particular interest here because it allows the overall quality of a given cylinder to be checked at a relatively low cost compared to X-Ray Tomography. With ultrasonic C-scan, the through thickness attenuation contained inside an entire cylinder can be investigated. However, the results that are obtained are only qualitative and not quantitative. A Sofratest ultrasonic inspection system was used to measure through thickness attenuation using 2 MHz focused transducers by placing the cylinder on a rotating table in a water tank. The attenuation levels provide a rapid indication of the overall quality in terms of voids. Results are shown in Figure 7, in which low attenuations levels are shown in red and high attenuation levels are shown in blue and black. It may be noted that the colour scales are different for the three cylinders.

Figure 7: Results from Ultrasonic C-scans of (a) C/Epoxy [$\pm 55^\circ$] (b) C/PA6 [$\pm 55^\circ$] (c) C/PA6 [$0^\circ/\pm 88^\circ$]

Based on experience [21], high levels of through thickness attenuation (over 20dB) usually correspond to the presence of significant voids. On the other hand, low levels of attenuation (below 10dB) indicate a good cylinder quality. These ultrasonic C-scans highlight two main results. First, it is shown that the C/Epoxy cylinder, Figure 7.a, has high localized levels of attenuation, meaning that there are defects at these locations. On the contrary, the carbon/polyamide 6 cylinders are of very good quality (the attenuation scale is much smaller, below 8dB), Figure 7.b and Figure 7.c. The voids are mostly localised at the end of the two thermoplastic cylinders (in the reinforcements for the one laid at [$0^\circ/\pm 88^\circ$]). Concerning the [$\pm 55^\circ$] cylinder, one defect is found all along the cylinder at an attenuation value of approximately 5dB. This corresponds to a groove induced by the mandrel. Indeed, the mandrel used to make the C/PA6 composite cylinder at [$\pm 55^\circ$] is a two-shell mandrel that allows easy removal after manufacture. This results in a shallow defect, which may affect the implosion behaviour and will be investigated later. These ultrasonic inspection results show that the thermoplastic composite cylinders that were manufactured by L ATP are of excellent quality in terms of voids compared to the C/Epoxy cylinder processed by wet filament winding. These results were confirmed by X-ray Tomography. Example of tomography results are presented in Figure 8. In these two pictures, voids are highlighted in black and show a much higher void level within the C/Epoxy cylinder compared with the C/PA6 cylinder.

Figure 8: X-ray tomography (Voxel: 12 μ m) performed on the (a) C/Epoxy cylinder and (b) C/PA6 [$\pm 55^\circ$] cylinder

3.2. Mechanical tests

3.2.1. Axial compression tests

Axial compression tests were performed on the three cylinders to obtain the elastic properties (moduli and Poisson's ratios) along the axial direction of the cylinders. Results from these tests are presented in Table 4 and are compared with the prediction calculated with laminate theory using Tables 3 and data from the literature for C/Epoxy.

Table 4 : *Elastic properties measured on the three cylinders and theoretical prediction using laminate theory*

These results show a good correlation between the experimental and theoretical axial modulus and Poisson's ratio for the different sequences. Therefore, these results can be used later to predict the implosion pressures.

3.2.2. Implosion tests

Once the quality and the elastic properties of the two cylinders were checked, implosion tests were performed in a hyperbaric chamber. It may be noted that the cylinders were partially filled with water to limit the shock wave at implosion, that can damage the pressure vessel.

3.2.2.1. Implosion test on C/Epoxy cylinder wound at [$\pm 55^\circ$]

The carbon/epoxy reference cylinder imploded at a pressure of 77.2 MPa (772 bar). The strain gauge data along the axial and hoop directions are respectively presented in Figure 9.a and Figure 9.b as a function of applied hydrostatic pressure.

Figure 9: *Change in strain as a function of pressure (a) Axial strain and (b) Hoop strain for the C/Epoxy cylinder wound at [$\pm 55^\circ$]*

The strains at failure in the axial and hoop directions are respectively -7000 microstrain and -3200 microstrain. It is worth noting that a significant drop in hoop compressive strains occurred at approximately 500 bar, however, it had no impact on the structural integrity of the cylinder. In order to identify the failure mode of the composite cylinder (buckling or material failure), the strains were then plotted radially as a function of the hoop angle, presented in Figure 10.

Figure 10: *Radial plot of the hoop strains in the C/Epoxy cylinder wound at $[\pm 55^\circ]$*

The black plot represents the compressive strain response just before implosion. An elliptical shape is identified, suggesting that the failure mode was overall buckling (mode II) of the C/Epoxy cylinder. These C/epoxy cylinders are used in applications down to 4500 meters (around 450 bars). Therefore, a safety factor of 1.7 is used when working at 450 bars compared to the implosion test pressure. This first implosion test represents the implosion pressure reference that is targeted for the thermoplastic composite cylinders.

3.2.2.2. Implosion test on C/PA6 cylinder laid at $[\pm 55^\circ]$

The $[\pm 55^\circ]$ C/PA6 cylinder was tested in the pressure vessel and imploded at 209 bar, which is much lower than the C/epoxy reference. The strain responses along the axial and hoop directions are plotted in Figure 11.a and Figure 11.b.

Figure 11: *Change in strain as a function of pressure (a) Axial strain and (b) Hoop strain for the C/PA6 cylinder wound at $[\pm 55^\circ]$*

Unlike the strain responses observed on the C/epoxy cylinder, considerable scatter is observed in the axial and hoop directions. The strain gauges all seem to diverge at a pressure slightly above 100 bar and the failure mode appears to be buckling which starts early in the test. From these plots, it is clear that the strains obtained for the $[\pm 55^\circ]$ C/PA6 cylinder are much higher (around 5000 microstrain at 200 bar) than for the C/Epoxy counterpart (around 1000 microstrain at 200 bar). There are several possible explanations. The first one is associated with an early plasticisation of the PA6 matrix. There are almost no fibres in the hoop direction so matrix yielding will lead to failure. The second might be associated with the non circular/elliptical shape of the

C/PA6 cylinder. A short study has been performed concerning the effect of these geometrical defects on the implosion strength. It is found in the Appendix.

Due to the presence of these defects, it was decided to work with a different mandrel for the optimized cylinder, in order to limit geometrical imperfections. Also, as stated earlier, the $[\pm 55^\circ]$ sequence is not an optimized sequence for hydrostatic pressure, so an alternative sequence was used $[0^\circ/\pm 88^\circ]$.

3.2.2.3. Implosion test on C/PA6 cylinder laid at $[0^\circ/\pm 88^\circ]$

The third cylinder, produced with a $[0^\circ/\pm 88^\circ]$ lay-up, imploded at a pressure of 610 bar. The axial and hoop strain recordings as a function of pressure are respectively presented in Figure 12.a and Figure 12.b. It may be noted that the strain gauge located at 135° failed during the manipulation of the cylinder before test.

Figure 12: *Change in strain as a function of pressure (a) Axial strain and (b) Hoop strain for the C/PA6 cylinder laid at $[0^\circ/\pm 88^\circ]$*

Unlike the first cylinders' strain responses, the plots presented in Figure 11 behave in an almost perfectly linear manner until a sudden failure occurred at 610 bar. This would suggest that material failure occurred rather than buckling, which is confirmed by the radial plot shown in Figure 13 where the change in strains is quite circular until failure. The strain responses do not tend towards an elliptical shape at failure, so it suggests a different failure mode (compression failure) for this thermoplastic cylinder with the optimized sequence. Also, the failure strains are very similar in the axial and hoop directions, suggesting that the modified stacking sequence is effective. The hoop strains achieved are a little higher than those at failure in the carbon/epoxy cylinder which was slightly thicker.

Figure 13: *Radial plot of the hoop strains in the for the C/PA6 cylinder laid at $[0^\circ/\pm 88^\circ]$*

The results were then compared to the finite element calculation results. The response in terms of strains as a function of hydrostatic pressure until failure is presented in Figure 14.

Figure 14: *Experimental hoop strains compared with the finite element calculations*

The results show an excellent agreement between the experimental data and the finite element prediction. The optimized sequence $[0^\circ/\pm 88^\circ]$ is much stiffer than the previous one $[\pm 55^\circ]$, so it increased the buckling pressure up to 1348 bar, which is consistent with the fact that material failure occurred here rather than buckling, Figure 15.a.

In addition, the in-plane compressive stresses (σ_{11}) within the tube at 610 bar are shown in Figure 15.b and were found to be close to 450 MPa, which is relatively low. For comparison, uniaxial compression tests performed on unidirectional specimens manufactured by press forming in [39] gave results slightly above 500 MPa, quite close to the values shown in Figure 15.b.

Figure 15 : (a) *Mode II buckling mode obtained at a pressure of 1348 bar* (b) *Through thickness compressive stress at 610 bar (inner wall at 0 mm)*

The three cylinders after implosion are shown in Figure 16. It should be kept in mind that for each condition of interest, only one cylinder was tested to implosion. From a reproducibility point of view, it would clearly have been preferable to perform at least three tests per condition; however, manufacturing and testing such cylindrical structures is both expensive and time-consuming. It may be noted that for the C/epoxy cylinders, many other tests have been performed in the past at Ifremer. These included a series on cylinders of the same thickness from the same supplier but of different lengths. These were 1.2 meters long, i.e. the actual length of the cylinders used today at Ifremer for deep sea applications. Considering that the implosion of the 600 mm long cylinder was due to buckling, it is thought that for a longer cylinder, implosion pressures would be lower. However, this was not the case because those cylinders imploded at 886 and 684 bar. This underlines the fact that in these intermediate thickness-to-diameter ranges, it is very difficult to define a failure criterion, either due to buckling or material failure. The experience from the World Wide Failure Exercise emphasised this conclusion [12].

Figure 16: *Composite cylinders after implosion tests - From left to right (i) C/PA6 $[\pm 0/88]$ (ii) C/PA6 $[\pm 55]$ (iii) C/Epoxy $[\pm 55]$*

4.2. Effect of water aging

Water absorption in polyamide 6 has been widely studied in the literature, however, there are several questions concerning the modelling of the water diffusion, especially for thick structural parts, which is of particular interest here. It has been shown several times in the literature that Polyamide 6 is a particularly hydrophilic material when immersed in water, as it absorbs up to 10 % of water at 20°C [40]. This significant water absorption induces a large **reduction** in the glass transition temperature that drops from 66°C down to -10°C when the PA6 absorbs 10% of water [37]. This has a significant effect on the mechanical properties [38]. It induces large changes within the material that goes from the glassy state to the rubbery state. Difficulties have been highlighted in the literature concerning the modelling of such a behaviour in terms of water diffusion. **This was studied within the current** project, in order to be able to model **the water profile** based on physical considerations. A model was recently proposed by the authors concerning this, using a classical Arrhenius law when the material is in the glassy state and the free volume theory when the material is in the rubbery state. More details can be found in [37]. However, this model was developed for the neat Polyamide 6 and not for composite materials, so it has been extended to composite materials using homogenisation equations described in the literature [41] and validated based on the water diffusion data obtained by the authors in [39]. **This extension to composite materials is based on unidirectional composites materials being considered to be transversely isotropic. Two diffusion coefficients D_1 and D_2 corresponding respectively to longitudinal and transverse diffusion, are needed. D_1 is taken as the diffusion coefficient of the matrix, as stated by Kondo and Taki [42]. Then, because of the transverse isotropy, the directions 2 and 3 (through thickness) are considered equal. Although the diffusion coefficient along the fibre direction D_1 is most often taken as that of the resin, the transverse diffusion coefficient is much more controversial. Most studies consider that the transverse diffusion coefficient D_2 corresponds to the diffusion coefficient of the resin reduced by a factor that lies between 0 and 1. Here, a factor of 0.3 was used and the diffusion coefficient of the resin at 15°C was taken from [37]. The water content at saturation used in the calculation was determined by weight gain measurements performed on C/PA6 specimens of the same material at 15°C in sea water, see [43]. Based on these input values the water diffusion profile in a thick composite cylinder immersed at 15°C in sea water for several years was modelled. Results are shown in Figure 16.**

Figure 16 : *Water distributions through the thickness of the C/PA6 cylinder (12 mm thick) for different immersion times and immersed in sea water at 15°C (inner wall at 0 mm)*

This figure shows the water profiles through the thickness of the cylinder for different immersion times (1, 2, 5, 10, 25 and 100 years). After two years, we can see that only 3 mm of the total thickness of the cylinder is affected by water, which suggests that the effect of water may be limited after 2 years but will affect the long term durability. In addition, when the profiler is immersed in deep water (< 2000 meters), the temperature of the ocean is close to 4°C, which suggests the water diffusion will be even slower under these conditions. The model results also represent a worst case scenario for the cylinder as an external coating will generally be applied to protect the cylinder. These results suggest that despite the sensitivity of polyamide 6 to water, it could provide a low cost thermoplastic composite matrix for deep sea applications

5. Conclusion

The aim of this paper was to study the implosion performance of thermoplastic composite cylinders manufactured by LATP compared to the filament wound C/Epoxy reference used today at Ifremer. First, the quality of these cylinders was checked using Ultrasonic C-scan and X-ray tomography. Results from ultrasonic C-scan showed high levels of attenuation (>20dB) in the C/Epoxy cylinder while very low attenuation levels were found in the C/PA6 cylinder (<8dB). These results indicate that the thermoplastic composite cylinder is of a much better quality in terms of voids than the thermoset counterpart. These results were also confirmed by X-ray tomography. Results from finite element analysis showed a good correlation with the axial loading and pressure testing results. For the two cylinders reinforced with fibres at $[\pm 55^\circ]$ a higher implosion pressure was achieved for the C/Epoxy reference, at 772 bar. The C/PA6 stacking sequence was then optimized to $[0^\circ/\pm 88^\circ]$, which provides a much stiffer behaviour than the $[\pm 55^\circ]$ angle. This cylinder imploded at 610 bar. Finally, these tests show that it is possible to use carbon fibre reinforced PA6 cylinders for underwater applications at depths down to 4000 meters (with a safety factor of 1.5), but further study is needed to achieve equivalent performance to the carbon/epoxy cylinders.

Appendix

This appendix presents the results from numerical modelling to investigate the effect of geometrical defects on the implosion strength for the C/PA6 cylinder laid at $[\pm 55^\circ]$. Any circular variability, either circularity

or coaxiality, has a strong effect on the critical buckling load [7]. These two parameters were measured on both cylinders wound at $[\pm 55^\circ]$ and results are presented in Table A.

Table A : *Concentricity and coaxiality of the composite cylinders wound at $\pm 55^\circ$*

Results show much higher concentricity and coaxiality variations for the thermoplastic cylinder. These are due to the two-shell mandrel used to manufacture this tube, which induces a significant groove (flat surface on the inner wall) along the length of the cylinder (as shown on Figure Aa). Results from the FE calculations indicate that as more pronounced geometrical defects are included (groove induced by the mandrel, cylindricality and coaxiality variations), the imploding buckling pressure decreases dramatically. When considering a perfectly circular cylinder, the implosion pressure was far above 700 bar. Then, when the groove (a flat surface of 10 mm along the tube) was included in the model, Figure A.a. it decreased down to 630 bar and changed the buckling mode to mode III, Figure A.b.

Figure A: *(a) Schematic representation of the groove induced by the two shell mandrel (b) Results from finite element calculations while considering the groove*

A second investigation focused on a local reduction of the diameter of the tube by 1 mm, in order to obtain an elliptical shape, Figure B.a, and indicated that the buckling pressure decreased down to 159 bar, Figure B.b. Also, strain responses from geometry variation calculations have shown that the minimum and maximum strains around the perimeter of the cylinder are very different, due to early mode III buckling, which could explain the significant scatter observed on Figure 11.b and observed on Figure A.

Figure B *(a) Schematic representation of the groove induced by the two shell mandrel (b) Results from finite element calculations while considering the groove combined with an ovalization of the cylinder*

These results show that taking account of geometry imperfections in the model has a very significant effect on the implosion pressure. When manufacturing composite tubes subjected to external pressure (compression loading), it is essential to limit geometrical defects, as they have much a much greater effect than for applications where composite tubes are subjected to internal pressures (tensile loading).

Acknowledgements

The authors acknowledge the contribution of the Carnot Institutes IFREMER-EDROME and CETIM for funding part of this study. At Ifremer, grateful thanks go to Christophe Peyronnet, Benoit Bigourdan, Patrick Beriet, Arnaud Le Moan, Nicolas Lacotte, Mickaël Premel Cabic and Luc Riou for their help concerning the implosion tests performed at Ifremer and the Ultrasonic C-Scans. At the CETIM, the work of Didier Mastain and Benoit Courtemanche concerning the processing of the C/PA6 cylinder is also gratefully acknowledged.

Data availability

The raw/processed data required to reproduce these findings cannot be shared at this time as the data also forms part of an ongoing study.

References

- [1] Smith, C. S. (1991). Design of submersible pressure hulls in composite materials. *Marine structures*, 4(2), 141-182.
- [2] Stevenson, P., Graham, D., & Clayson, C. (1998). The mechanical design and implementation of an autonomous submersible. *Underwater Technology*, 23(1), 31-41.
- [3] Stachiw, J. D., & Frame, B. (1988). Graphite-Fiber-Reinforced Plastic Pressure Hull Mod 2 for the Advanced Unmanned Search System Vehicle (No. NOSC-TR-1245). NAVAL OCEAN SYSTEMS CENTER SAN DIEGO CA.
- [4] Graham-Jones, J., & Summerscales, J. (Eds.). (2015). *Marine applications of advanced fibre-reinforced composites*. Woodhead Publishing.
- [5] Starbuck, J. M., & Blake, H. W. (1994). Failure of thick composite cylinders subjected to external hydrostatic pressure. In *Compression Response of Composite Structures*. ASTM International.
- [6] Graham, D. (1995). Composite pressure hulls for deep ocean submersibles. *Composite Structures*, 32(1-4), 331-343.
- [7] Tsouvalis, N. G., Zafeiratou, A. A., & Papazoglou, V. J. (2003). The effect of geometric imperfections on the buckling behaviour of composite laminated cylinders under external hydrostatic pressure. *Composites Part B: Engineering*, 34(3), 217-226.

- [8] Messenger, T. (2001). Buckling of imperfect laminated cylinders under hydrostatic pressure. *Composite structures*, 53(3), 301-307.
- [9] Pinto, M., Gupta, S., & Shukla, A. (2015). Study of implosion of carbon/epoxy composite hollow cylinders using 3-D digital image correlation. *Composite Structures*, 119, 272-286.
- [10] Javier, C., Matos, H., & Shukla, A. (2018). Hydrostatic and blast initiated implosion of environmentally degraded Carbon-Epoxy composite cylinders. *Composite Structures*.
- [11] Messenger, T., Pyrz, M., Gineste, B., & Chauchot, P. (2002). Optimal laminations of thin underwater composite cylindrical vessels. *Composite Structures*, 58(4), 529-537.
- [12] Hinton, M. J., Soden, P. D., & Kaddour, A. S. (1996). Strength of composite laminates under biaxial loads. *Applied Composite Materials*, 3(3), 151-162.
- [13] Soden, P. D., Hinton, M. J., & Kaddour, A. S. (2004). Biaxial test results for strength and deformation of a range of E-glass and carbon fibre reinforced composite laminates: failure exercise benchmark data. In *Failure Criteria in Fibre-Reinforced-Polymer Composites* (pp. 52-96).
- [14] Soden, P. D., Kaddour, A. S., & Hinton, M. J. (2004). Recommendations for designers and researchers resulting from the world-wide failure exercise. In *Failure Criteria in Fibre-Reinforced-Polymer Composites* (pp. 1223-1251).
- [15] Hur, S. H., Son, H. J., Kweon, J. H., & Choi, J. H. (2008). Postbuckling of composite cylinders under external hydrostatic pressure. *Composite Structures*, 86(1-3), 114-124.
- [16] Moon, C. J., Kim, I. H., Choi, B. H., Kweon, J. H., & Choi, J. H. (2010). Buckling of filament-wound composite cylinders subjected to hydrostatic pressure for underwater vehicle applications. *Composite Structures*, 92(9), 2241-2251.
- [17] Comer, A. J., Ray, D., Obande, W. O., Jones, D., Lyons, J., Rosca, I., ... & McCarthy, M. A. (2015). Mechanical characterisation of carbon fibre-PEEK manufactured by laser-assisted automated-tape-placement and autoclave. *Composites Part A: Applied Science and Manufacturing*, 69, 10-20.
- [18] Jar, P. Y., Mulone, R., Davies, P., & Kausch, H. H. (1993). A study of the effect of forming temperature on the mechanical behaviour of carbon-fibre/peek composites. *Composites science and technology*, 46(1), 7-19.
- [19] Davies, P., Cantwell, W. J., Jar, P. Y., Richard, H., Neville, D. J., & Kausch, H. H. (1991). Cooling rate effects in carbon fiber/PEEK composites. In *Composite Materials: Fatigue and Fracture (Third Volume)*. ASTM International.

- [20] Gruber, M. B., Lamontia, M. A., Smoot, M. A., & Peros, V. (1995). Buckling performance of hydrostatic compression-loaded 7-inch diameter thermoplastic composite monocoque cylinders. *Journal of Thermoplastic Composite Materials*, 8(1), 94-108.
- [21] Davies, P., Riou, L., Mazeas, F., & Warnier, P. (2005). Thermoplastic composite cylinders for underwater applications. *Journal of Thermoplastic Composite Materials*, 18(5), 417-443.
- [22] Sparks, C. P. (1986). Lightweight composite production risers for a deep water tension leg platform.
- [23] Baldwin, D. D., Newhouse, N. L., Lo, K. H., & Burden, R. C. (1997, January). Composite production riser design. In *Offshore technology conference*. Offshore Technology Conference.
- [24] Storhaug, T. U. R. I. D., STJERN, G., PAULSHUS, B., & SLAMA, M. (2001). Significant achievements in composite technology in 2001; Qualification and testing of Composite tethers and risers for Ultra seep water. *Proc. Deep offshore Technology, DOT*.
- [25] Salama, M. M., Stjern, G., Storhaug, T., Spencer, B., & Echtermeyer, A. (2002, January). The first offshore field installation for a composite riser joint. In *Offshore technology conference*. Offshore Technology Conference.
- [26] Ochoa, O. O. (2006). Composite riser experience and design guidance.
- [27] Thermoplastic piping systems - Non metallic materials, DNVGL-CP-0072, December 2015
- [28] Airborne website: <http://airborne-oilandgas.com/>
- [29] Magma website: <https://www.magmaglobal.com/technology/>
- [30] Dirk, H. J. L., Ward, C., & Potter, K. D. (2012). The engineering aspects of automated prepreg layup: History, present and future. *Composites Part B: Engineering*, 43(3), 997-1009.
- [31] Lamontia, M. A., Gruber, M. B., Tierney, J. J., Gillespie Jr, J. W., Jensen, B. J., & Cano, R. J. (2009, March). In situ thermoplastic ATP needs flat tapes and tows with few voids. In *30th International SAMPE Europe Conference*, Paris.
- [32] Khan, M. A., Mitschang, P., & Schledjewski, R. (2010). Identification of some optimal parameters to achieve higher laminate quality through tape placement process. *Advances in polymer technology*, 29(2), 98-111.
- [33] Lan, M., Cartié, D., Davies, P., & Baley, C. (2015). Microstructure and tensile properties of carbon–epoxy laminates produced by automated fibre placement: Influence of a caul plate on the effects of gap and overlap embedded defects. *Composites Part A: Applied Science and Manufacturing*, 78, 124-134.

- [34] Mazumdar, S. K. (1994). Automated manufacturing of composite components by thermoplastic tape winding and filament winding (Doctoral dissertation, Concordia University).
- [35] Qureshi, Z., Swait, T., Scaife, R., & El-Dessouky, H. M. (2014). In situ consolidation of thermoplastic prepreg tape using automated tape placement technology: Potential and possibilities. *Composites Part B: Engineering*, 66, 255-267.
- [36] Stokes-Griffin, C. M., & Compston, P. (2015). The effect of processing temperature and placement rate on the short beam strength of carbon fibre-PEEK manufactured using a laser tape placement process. *Composites Part A: Applied Science and Manufacturing*, 78, 274-283.
- [37] Arhant, M., Le Gac, P. Y., Le Gall, M., Burtin, C., Briançon, C., & Davies, P. (2016). Modelling the non Fickian water absorption in polyamide 6. *Polymer Degradation and Stability*, 133, 404-412.
- [38] Le Gac, P. Y., Arhant, M., Le Gall, M., & Davies, P. (2017). Yield stress changes induced by water in polyamide 6: Characterization and modeling. *Polymer Degradation and Stability*, 137, 272-280.
- [39] Arhant, M., Le Gac, P. Y., Le Gall, M., Burtin, C., Briançon, C., & Davies, P. (2016). Effect of sea water and humidity on the tensile and compressive properties of carbon-polyamide 6 laminates. *Composites Part A: Applied Science and Manufacturing*, 91, 250-261.
- [40] Silva, L., Tognana, S., & Salgueiro, W. (2013). Study of the water absorption and its influence on the Young's modulus in a commercial polyamide. *Polymer Testing*, 32(1), 158-164.
- [41] Dana, H. R., Perronnet, A., Fréour, S., Casari, P., & Jacquemin, F. (2013). Identification of moisture diffusion parameters in organic matrix composites. *Journal of Composite Materials*, 47(9), 1081-1092.
- [42] Kondo, K., & Taki, T. (1982). Moisture diffusivity of unidirectional composites. *Journal of Composite Materials*, 16(2), 82-93.
- [43] Pemberton, R., Summerscales, J., & Graham-Jones, J. (Eds.). (2018). *Marine Composites: Design and Performance*. Chapter 2: Thermoplastic matrix composites for marine applications. Woodhead Publishing, 31-53.

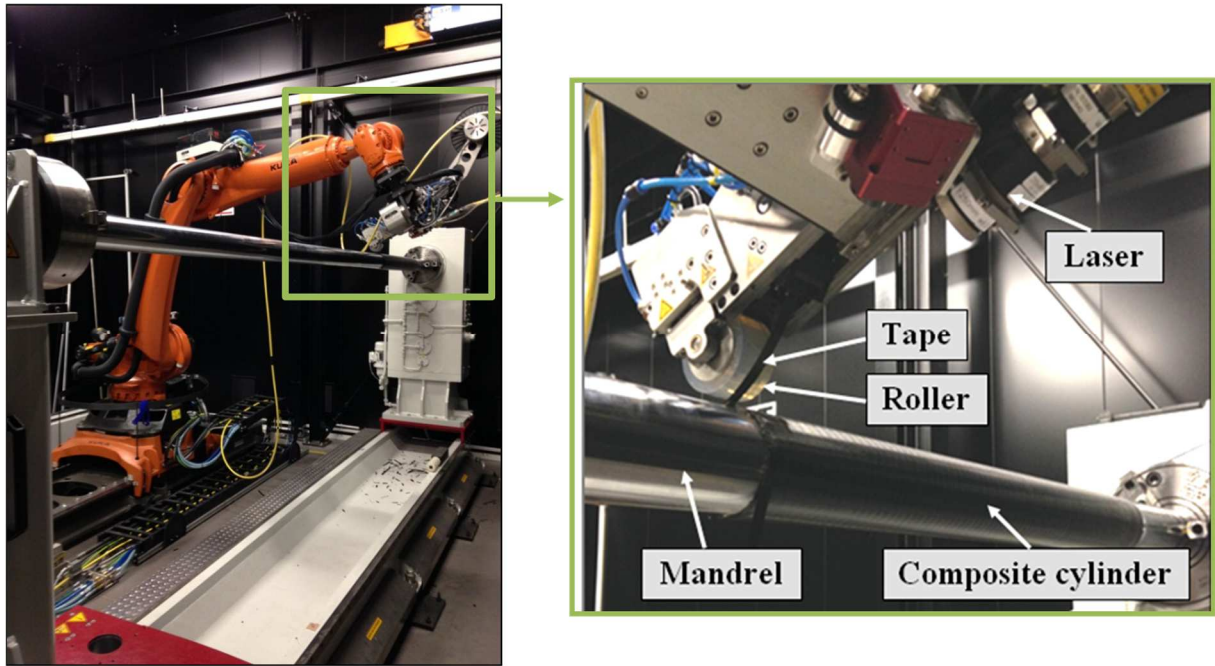


Figure 1 : C/PA6 Thermoplastic cylinder manufactured by LATP at CETIM composite manufacturing facility using Kuka robot and AFPT heating head

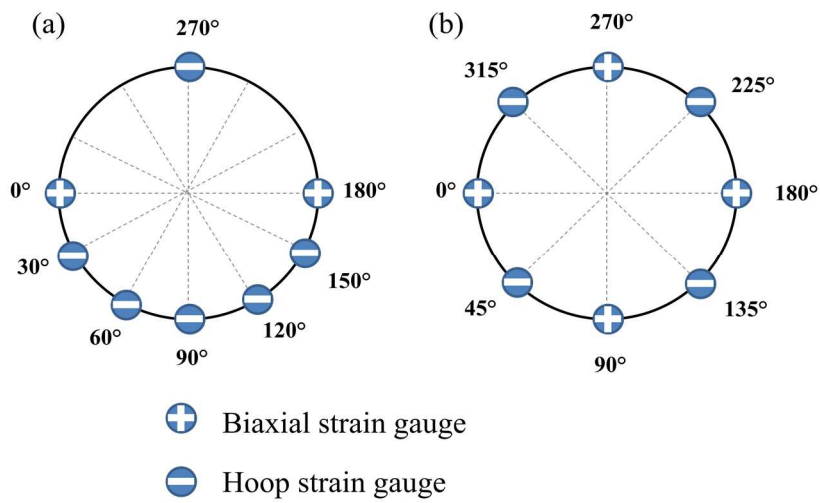


Figure 2: Strain gauge configurations used for the composite cylinders (a) C/Epoxy [$\pm 55^\circ$] and C/PA6 [$\pm 55^\circ$]
(b) C/PA6 [$0^\circ/\pm 88^\circ$]



Figure 3: Axial compression test performed on a C/PA6 thermoplastic cylinder



Figure 4 : 2400 bar pressure used for implosion test showing the 100 mm diameter C/PA6 cylinder just before test

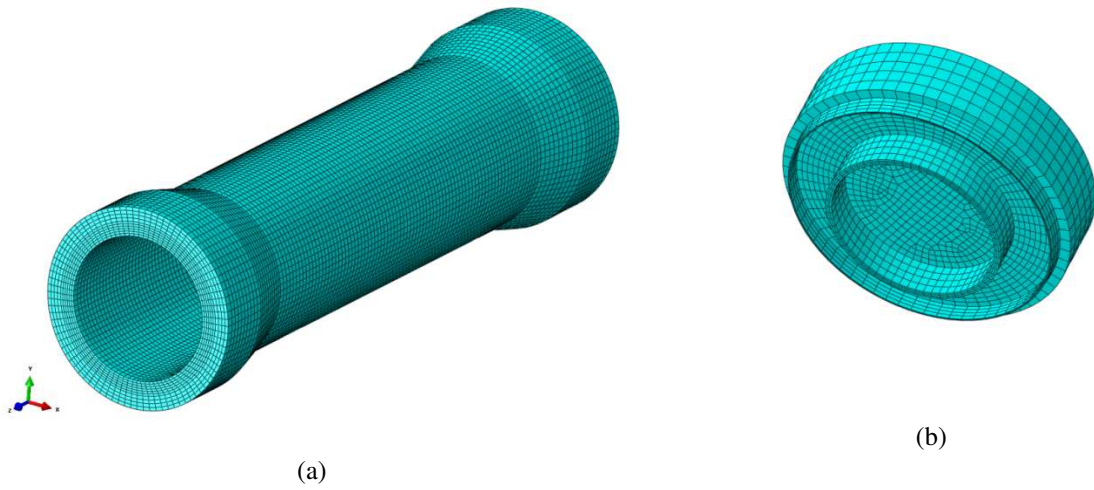


Figure 5: Mesh conditions using hexahedron elements for the $[0^\circ/\pm 88^\circ]$ composite cylinder, type C3D8R elements (a) Composite tube (b) End fixtures

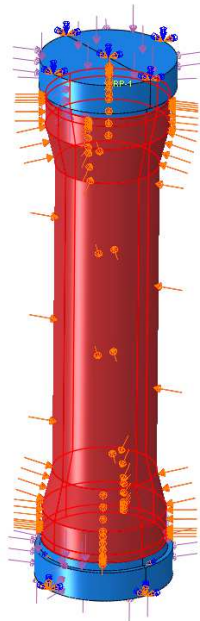


Figure 6: Pressure conditions used for modelling

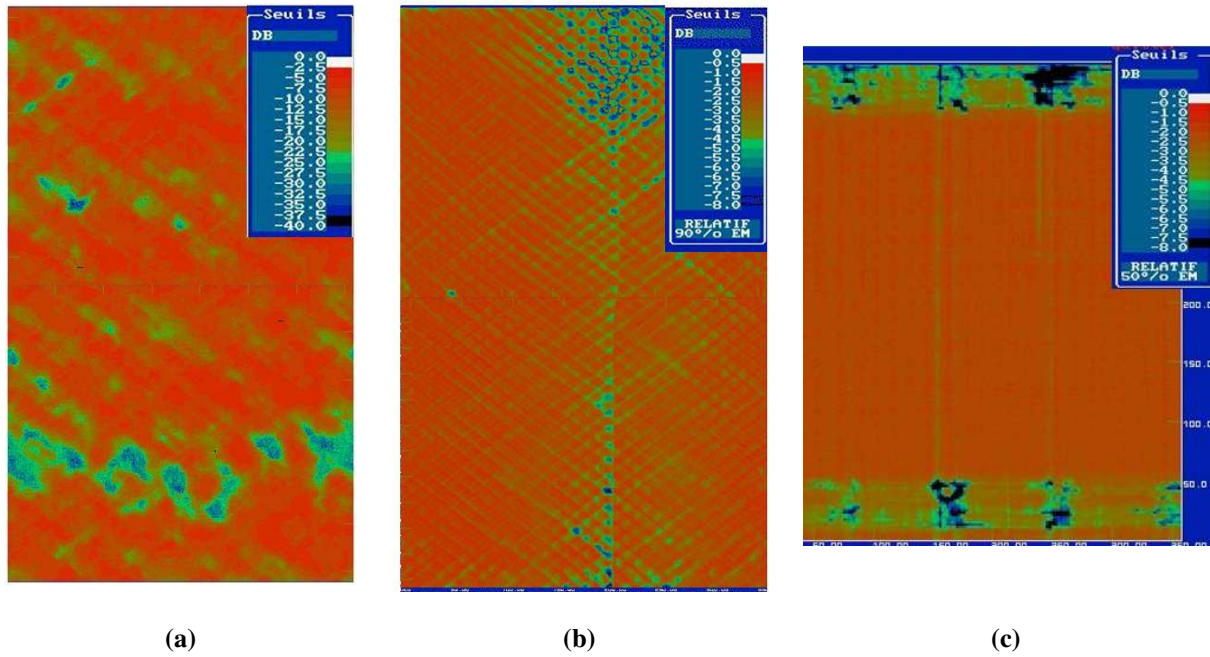


Figure 7: Results from Ultrasonic C-scans of (a) C/Epoxy [$\pm 55^\circ$] (b) C/PA6 [$\pm 55^\circ$] (c) C/PA6 [$0^\circ/\pm 88^\circ$]

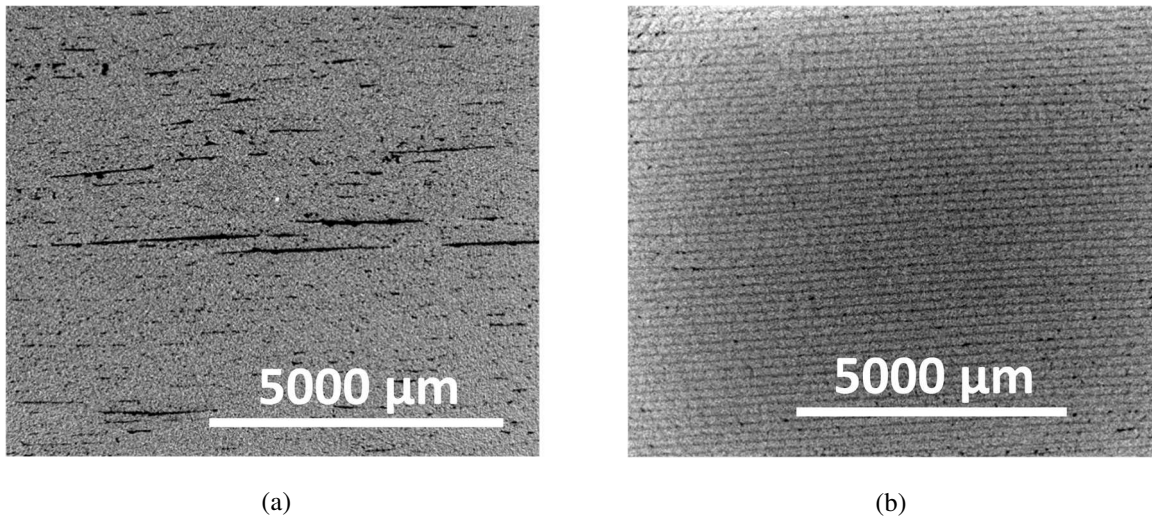


Figure 8: X-ray tomography (Voxel: $12\mu\text{m}$) performed on the (a) C/Epoxy cylinder and (b) C/PA6 [$\pm 55^\circ$] cylinder

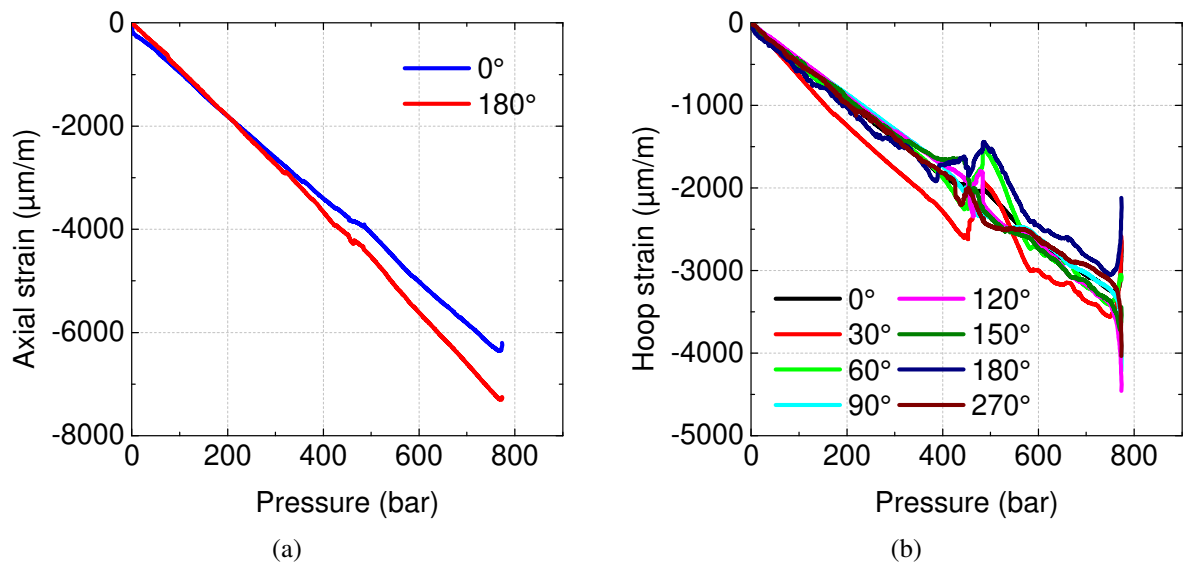


Figure 9 : *Change in strain as a function of pressure (a) Axial strain and (b) Hoop strain for the C/Epoxy cylinder wound at $[\pm 55^\circ]$*

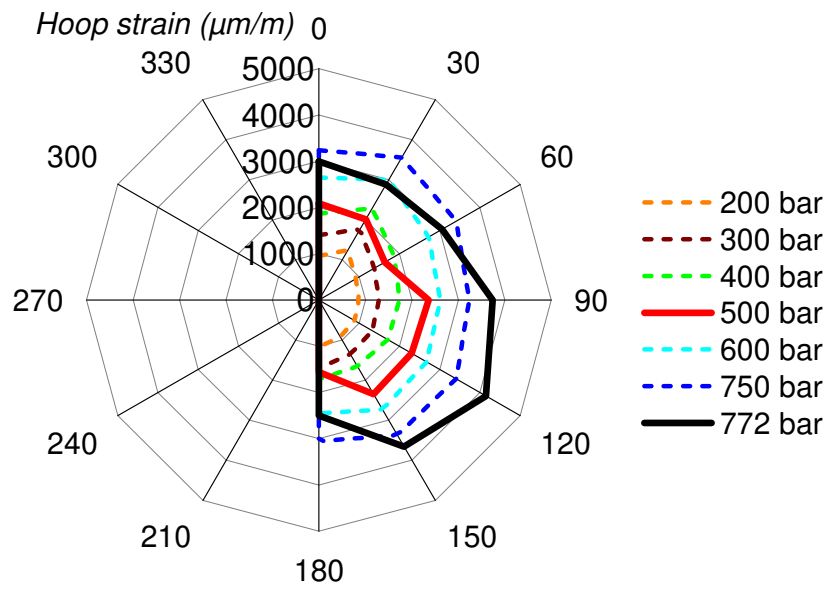


Figure 10: *Radial plot of the hoop strains in the C/Epoxy cylinder wound at $[\pm 55^\circ]$*

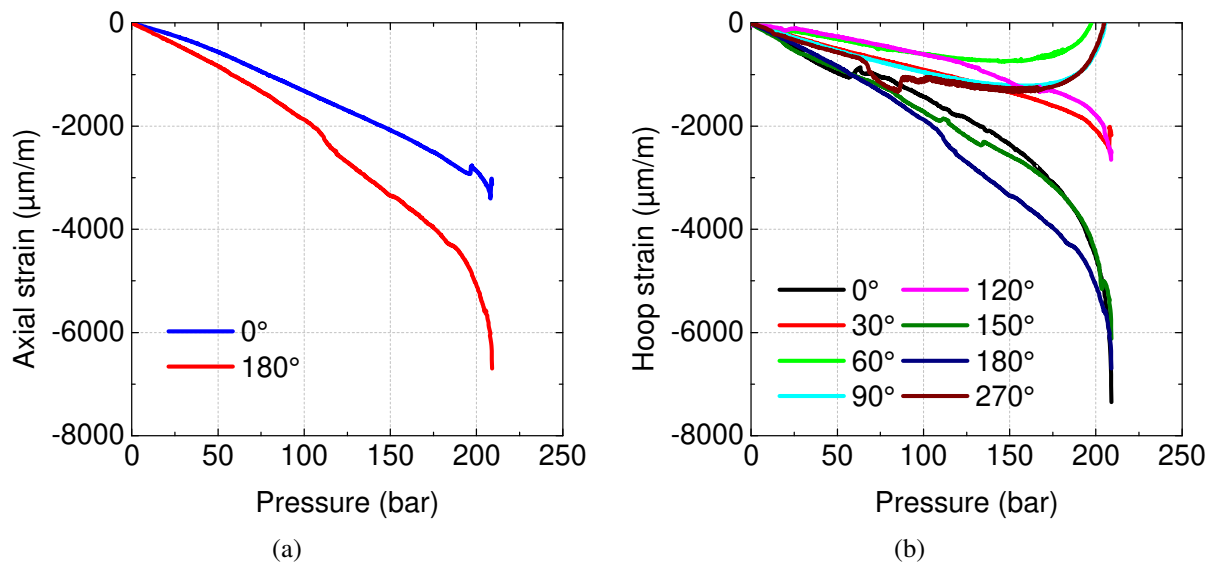


Figure 11 : *Change in strain as a function of pressure (a) Axial strain and (b) Hoop strain for the C/PA6 cylinder wound at $[\pm 55^\circ]$*

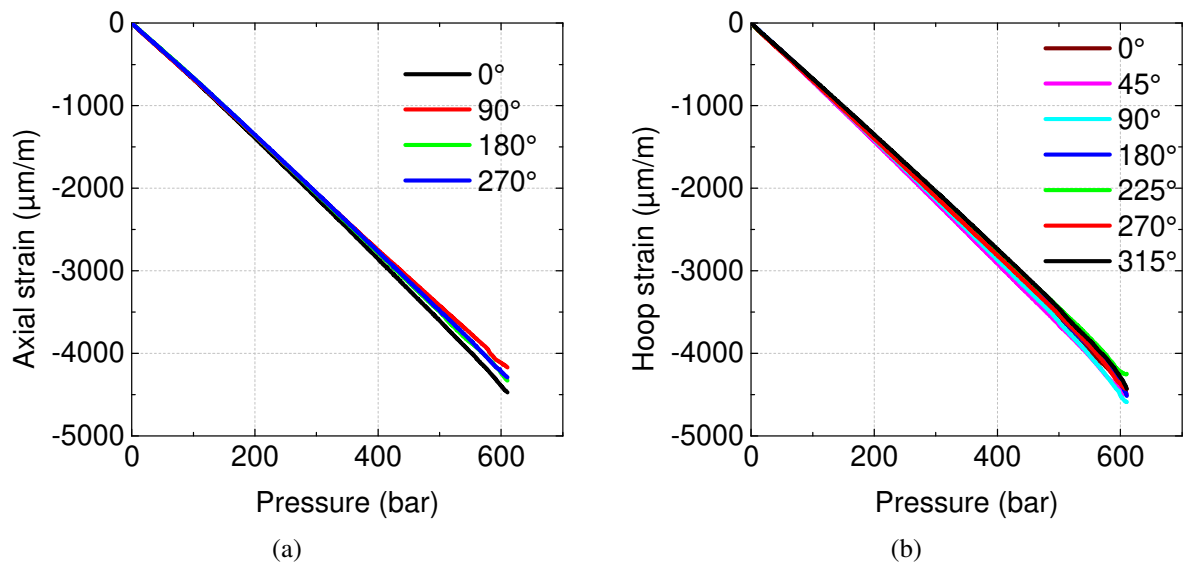


Figure 12: *Change in strain as a function of pressure (a) Axial strain and (b) Hoop strain for the C/PA6 cylinder laid at $[0^\circ/\pm 88^\circ]$*

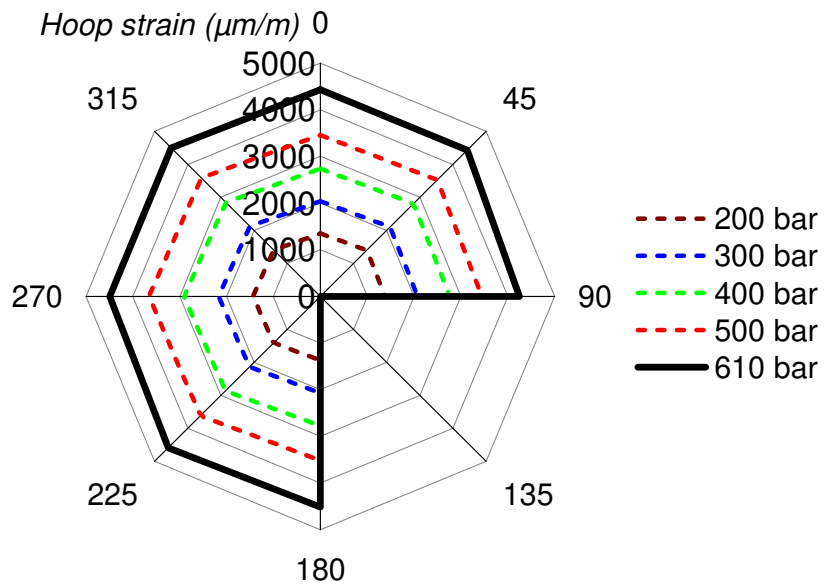


Figure 13: Radial plot of the hoop strains in the for the C/PA6 cylinder laid at $[0^\circ/\pm 88^\circ]$

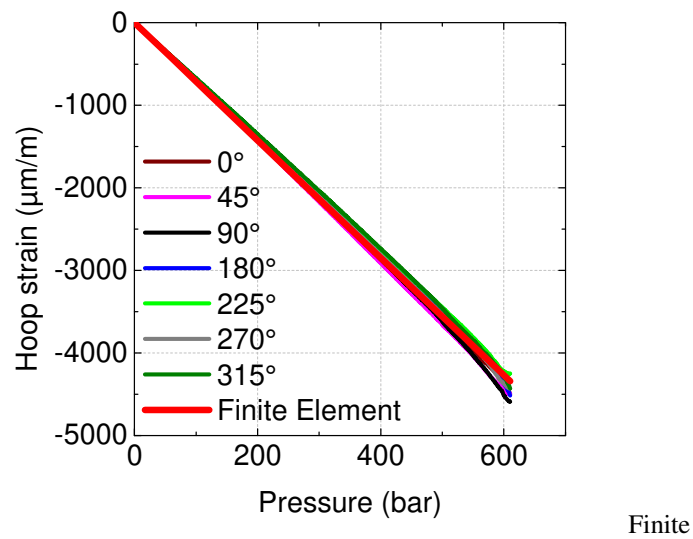
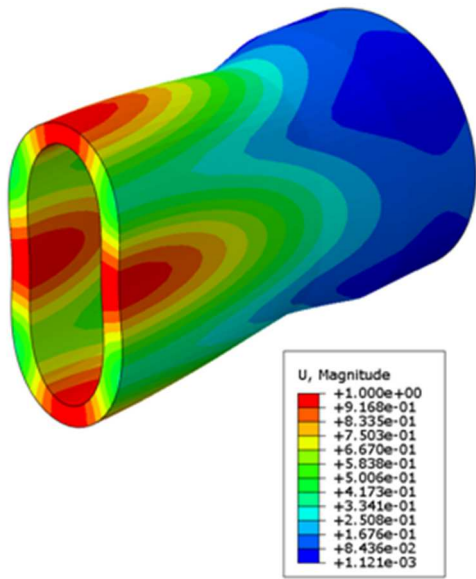


Figure 14: Experimental hoop strains compared with the finite element calculations



(a)

(b)

Figure 15 : (a) Mode II buckling mode obtained at a pressure of 1348 bar (b) Through thickness compressive stress at 610 bar (inner wall at 0 mm)



Figure 16: Composite cylinders after implosion tests - From left to right (i) C/PA6 [$\pm 0/88$] (ii) C/PA6 [± 55] (iii) C/Epoxy [± 55]

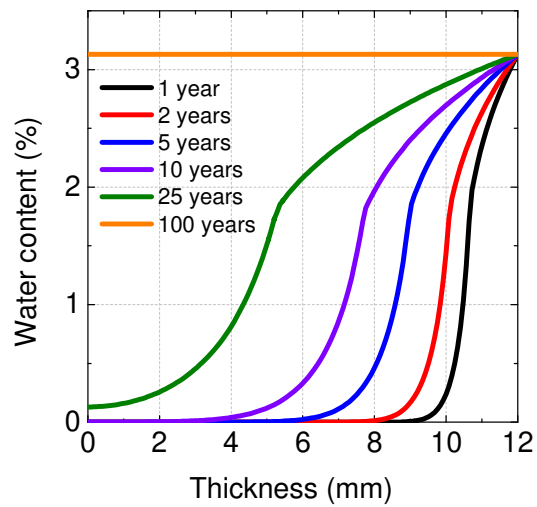


Figure 17 : Water distributions through the thickness of the C/PA6 cylinder (12 mm thick) for different immersion times and immersed in sea water at 15°C (inner wall at 0 mm)

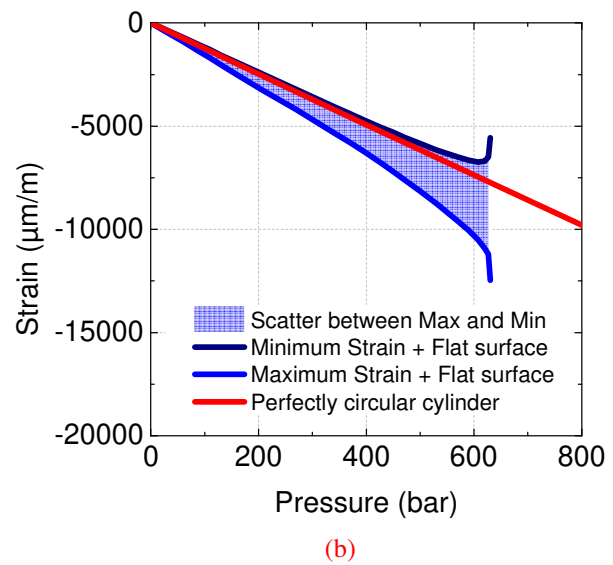
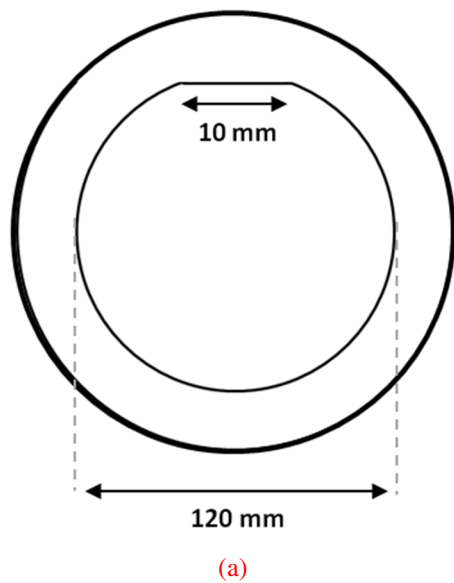
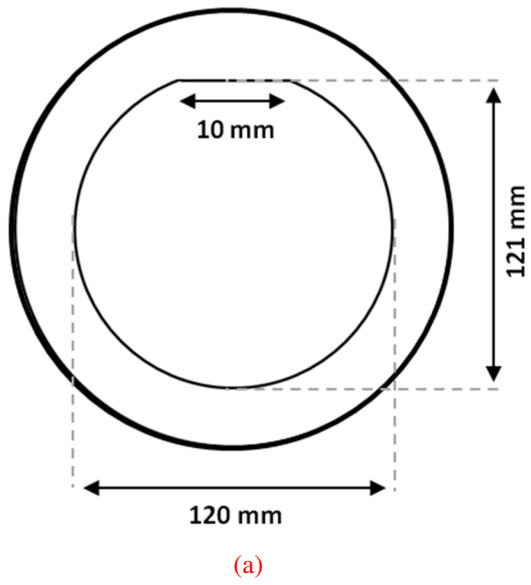


Figure A : (a) Schematic representation of the groove induced by the two shell mandrel (b) Results from finite element calculations while considering the groove



(b)

Figure B : (a) Schematic representation of the groove induced by the two shell mandrel (b) Results from finite element calculations while considering the groove combined with an ovalization of the cylinder

Table 1 : Dimensions and geometry of the cylinders tested during this work


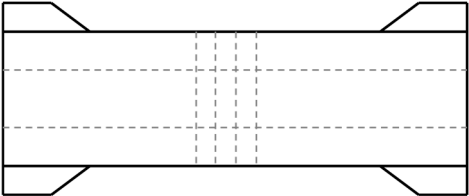
Tube	Length (mm)	Inner Diameter (mm)	Wall thickness (mm)	Cylinder shape
C/Epoxy [$\pm 55^\circ$] ₃₁	600	120	12.7	
C/PA6 [$\pm 55^\circ$] ₃₁	600	120	9.2	
C/PA6 [0/ $\pm 88^\circ$] ₂₆	500	100	12.1	

Table 2: Process parameters used for manufacturing thermoplastic composite cylinders

Material	Sequence	Laying speed (m/min)	Temperature (°C)	Roller pressure (bar)	
C/PA6	[$\pm 55^\circ$] ₃₁	18	280	2	
C/PA6	[0/ $\pm 88^\circ$] ₂₆	$\pm 88^\circ$	6.3	280	3
		0°	3.0	300	3

Table 3: Mechanical properties used in the modelling stage for the C/PA6 cylinders, from [37], *calculated using laminate theory, not measured

M_f (%)	V_f (%)	Void Content (%)	$E_{1\text{compression}}$ (GPa)	E_2 (GPa)	E_3 (GPa)*	ν_{12}	ν_{13}^*	ν_{23}^*	G_{12} (GPa)	G_{13} (GPa)*	G_{23} (GPa)*
60	48	2	89.7	5.8	5.8	0.36	0.36	0.4	2.4	2.4	2

Table 4 : Elastic properties measured on the three cylinders and theoretical prediction using laminate theory

Tube	Sequence	Experimental		Laminate Theory	
		E_z (GPa)	$\nu_{z\theta}$	E_z (GPa)	$\nu_{z\theta}$
C/Epoxy	[$\pm 55^\circ$] ₃₁	11.3	0.36	10.8	0.44

C/PA6	$[\pm 55^\circ]_{31}$	5.9	0.44	6.1	0.46
C/PA6	$[0^\circ/\pm 88^\circ]_{26}$	39.8	0.13	39.3	0.03

Table A : Concentricity and coaxiality of the composite cylinders wound at $\pm 55^\circ$

	Mean Diameter (mm)	Cylindricity variation (mm)	Coaxiality variation (mm)
C/Epoxy $\pm 55^\circ$	120.30	0.02	0.20
C/PA6 $\pm 55^\circ$	121.34	0.54	0.62